Engineering and Technology Journal
Journal homepage: https://etj.uotechnology.edu.iq

Design of a Sliding Mode Controller for a Prosthetic Human Hand's Finger

Hussein Sh. Majeed *, Saleem K. Kadhim , Alaa Abdulhady Jaber

Control and Systems Engineering Dept., University of Technology, Alsina'a Street, P.O Box 10066, Baghdad, Iraq.
*Corresponding author Email: 61366@student.uotechnology.edu.iq

HIGHLIGHTS

- The prosthetic finger is move by tendon instead of motor.
- The system is non-linear dynamic model.
- Sliding mode control can drive the model to desired position.
- Classical Sliding mode control suffers from chattering.

ARTICLE INFO

Handling editor: Muhsin J. Jweeg
Keywords:
Prosthetic finger;Tendon Driven; Modeling; Sliding mode control (SMC); Adaptive sliding mode control (ASMC)

ABSTRACT

In this research paper, the modeling and control of a tendon driven, instead of joint motors, prosthetic finger that mimics the actual human index finger were deliberated. Firstly, the dynamic model of the prosthetic finger is developed based on a 3-degree of freedom (DOF) articulated robot structure and utilizing the Lagrange equation. Then, the classical sliding mode control (CSMC) strategy was implemented to control the finger motion. To overcome the cons of CSMC, such as the chattering problem, an adaptive sliding mode controller (ASMC) was developed. MATLAB Simuphalange was used to perform the simulation after the necessary equations were derived. The obtained results showed that the ASMC superior to the CSMC in depressing the chattering and fast response.

1. Introduction

In our society, robots play an important role. They are currently commonly used for labor-intensive operations in various industrial applications that involve a high degree of precision and repetition. In the entertainment industry, robots can be used in the form of toys and animations. The role of robots in society is continually evolving. This research aims to bring them further into domestic aid, medicine, military, search, and rescue. The robot must perform only one particular task in many of these applications and be an engineered for a single operation. However, as robots' possible use increases, they will need to communicate with objects in their environments. The creation of end effectors that accumulate and use various objects as resources is an important challenge in robots' production. The human hand is considered to be the most dexterous end effector, with a total of 26 DOF [1]. The construction of a highly advanced prosthesis hand needs to deal with two significant problems: the development of a mechanical design that would permit enough movement freedom and how to build controllers be robust and capable of handling the associated mechanical design, which is commonly so complicated. The human body movement is based on the muscles that apply forces to the skeleton by the tendons. In the literature, with the robot and prosthetic hand, the human hand's motion system is commonly applied to imitate the natural movement [2].

The human hand tendon arrangements were tested to ensure that the robot's hands have the maximum total muscle strength requirements. From this analysis, it can be inferred that the robotic hand has force values highly related to that of the human hand. Weghe et al. [3] Created a human hand tested that was anatomically correct to determine its mechanism, function, and power. In recent years, many papers have investigated the serial robots assembled based on the tendon-driven mechanisms, which are composed of pulley-belt configurations. Kawanishi, et al. [4] have developed a system considering the fuzzy logic approach for fingertip position control of a 4 DOF tendon-driven robotic finger. The tendon's elasticity was also taken into consideration. Hristu et al. [5] made a comparison between the efficiency of fuzzy logic and traditional PID controllers for a multi-finger robotic hand. The aim was to control both the fingertip's position and the forces exerted on the fingertip. It was established that the fuzzy logic control approach superior to the PID controller. Muscles will exercise pulling effort only, and muscle forces are sent through the tendons to the finger bones. The muscles of the forearm stretch to the hand more than fifteen

http://doi.org/10.30684/etj.v40i1.1943
Received 07 December 2020; Accepted 24 April 2021; Available online 25 January 2022
2412-0758/University of Technology-Iraq, Baghdad, Iraq

tendons. When the finger is extended, one set of muscles and tendons exercise the finger's expanding motion, and a separate set of muscles and tendons create the bending motion. Tendon structure in hands is problematic and, however, leads to the high functionality of human hand movements through this sophisticated tendon arrangement. Hand tendons that lie at the back of the human hand straighten the fingers and flexor tendons and turn the fingers on the palm side of the hand. In this research, a 3-degree of freedom chain robot mechanism closely mimics the human index finger's size is modeled. On the palm and the back of the hand, the phalanges' tendon fixing points are reduced to three.

However, the considered problem in this work is the control of an under actuated finger, which is a very challenging task than the fully actuated one, and how to guarantee the overall stability of such a system. The work suggests first designing a classical sliding mode controller (CSMC), which is theoretically is able to reject the bounded matched perturbation altogether. The following points summarize the main steps that are conducted in this research to obtain this work's aim:

1) To analyze of dynamic model and state space representation of finger contact grasped object for the human prosthetic hand.
2) To the development of conventional sliding mode control (SMC) algorithm of the prosthetic finger.
3) To analyze the prosthetic finger's stability controlled by the conventional SMC scheme based on the sliding surface defined in the state space representation, the control action is responsible for maintaining and constructing the sliding motion.

2. Model development

Figure 1 represents the finger of a human prosthetic hand, on which the controller methods are applied. A prosthesis model of the two dimensions (2D) finger was considered a movie chain consisting of three cylindrical phalanges that mimic the inertial characteristics of the finger index's proximal, central and distal phalanges, as demonstrated in Figure 2. The articulations of the model to reflect the joint masses of the finger were supplemented with spherical components.

Based on Figure 2, where X and Y represent the displacement of the prosthetic finger while θ refers to the angular displacement of the philandering finger, the displacement equations are:

$$x_1 = l_1 \cos\theta_1 \tag{1}$$

$$y_1 = l_1 \sin\theta_1 \tag{2}$$

$$x_2 = l_1 \cos\theta_1 + l_2 \cos(\theta_1 + \theta_2) \tag{3}$$

$$y_2 = l_1 \sin\theta_1 + l_2 \sin(\theta_1 + \theta_2) \tag{4}$$

$$x_3 = l_1 \cos\theta_1 + l_2 \cos(\theta_1 + \theta_2) + l_3 \cos(\theta_1 + \theta_2 + \theta_3) \tag{5}$$

$$y_3 = l_1 \sin\theta_1 + l_2 \sin(\theta_1 + \theta_2) + l_3 \sin(\theta_1 + \theta_2 + \theta_3) \tag{6}$$

The linear velocity of the masses can be found as follows, where $\dot{\theta}$ is the angular velocity:

$$\dot{x}_1 = -l_1\dot{\theta}_1 \sin\theta_1 \tag{7}$$

$$\dot{y}_1 = l_1\dot{\theta}_1 \cos\theta_1 \tag{8}$$

$$\dot{x}_2 = -l_1\dot{\theta}_1 \sin\theta_1 - l_2(\dot{\theta}_1 + \dot{\theta}_2)\sin(\theta_1 + \theta_2) \tag{9}$$

$$\dot{y}_2 = l_1\dot{\theta}_1 \cos\theta_1 + l_2\left(\dot{\theta}_1 + \dot{\theta}_2\right)\cos(\theta_1 + \theta_2) \tag{10}$$

$$\dot{x}_3 = -l_1\dot{\theta}_1 \sin\theta_1 - l_2\left(\dot{\theta}_1 + \dot{\theta}_2\right)\sin(\theta_1 + \theta_2) - l_3\left(\dot{\theta}_1 + \dot{\theta}_2 + \dot{\theta}_3\right)\sin(\theta_1 + \theta_2 + \theta_3) \tag{11}$$

$$\dot{y}_3 = l_1\dot{\theta}_1 \cos\theta_1 + l_2\left(\dot{\theta}_1 + \dot{\theta}_2\right)\cos(\theta_1 + \theta_2) + l_3\left(\dot{\theta}_1 + \dot{\theta}_2 + \dot{\theta}_3\right)\cos(\theta_1 + \theta_2 + \theta_3) \tag{12}$$

$$v_1^2 = \dot{x_1^2} + \dot{y_1^2} = (-l_1\dot{\theta}_1 s_1)^2 + (l_1\dot{\theta}_1 c_1)^2 = l_1^2\dot{\theta}_1^2 \tag{13}$$

$$v_2^2 = \dot{x_2^2} + y_2^2 = \left(-l1s_1\dot{\theta_1} - l2s_{12}(\dot{\theta_1} + \dot{\theta_2})\right)^2 + \left(l1c_1\dot{\theta_1} + l2c_{12}(\dot{\theta_1} + \dot{\theta_2})\right)^2 \tag{14}$$

$$v_3^2 = \dot{x_3^2} + \dot{y_3^2} = \left(-l1s_1\dot{\theta_1} - l2s_{12}\left(\dot{\theta_1} + \dot{\theta_2}\right) - l3s_{123}\left(\dot{\theta_1} + \dot{\theta_2} + \dot{\theta_3}\right)\right)^2 + \left(l1c_1\dot{\theta_1} + l2c_{12}\left(\dot{\theta_1} + \dot{\theta_2}\right) + l3c_{123}\left(\dot{\theta_1} + \dot{\theta_2} + \dot{\theta_3}\right)\right)^2 \tag{15}$$

Figure 1: Prosthetic finger type InMoov Finger Starter

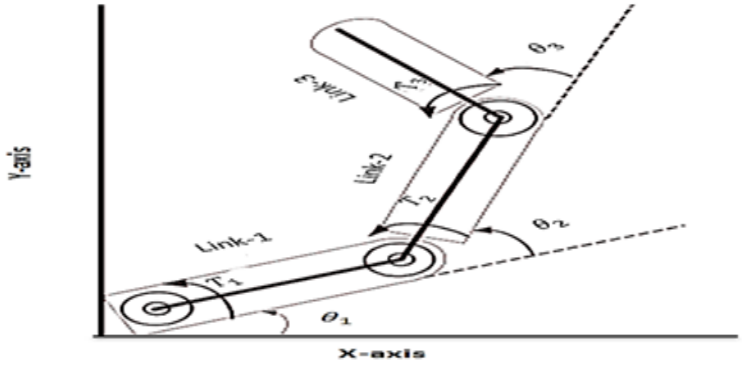

Figure 2: Schematic diagram of a three phalanges finger

However, the following equation can be used to find the total finger kinetic energy:

$$K = \frac{1}{2}m_1(v_1)^2 + \frac{1}{2}m_2(v_2)^2 + \frac{1}{2}m_3(v_3)^2 \tag{16}$$

Where m_1, m_2 and m_3 are the masses of the first, second, and third phalanges, respectively[6]. This gives the following equation:

$$K = \frac{1}{2}m_1 l_1^2\dot{\theta}_1^2 + \frac{1}{2}m_2\left(\left(-l1s_1\dot{\theta}_1 - l2s_{12}(\dot{\theta}_1+\dot{\theta}_2)\right)^2 + \left(l1c_1\dot{\theta}_1 + l2c_{12}(\dot{\theta}_1+\dot{\theta}_2)\right)^2\right) + \frac{1}{2}m_3\left(\left(-l1s_1\dot{\theta}_1 - l2s_{12}(\dot{\theta}_1+\dot{\theta}_2) - l3s_{123}(\dot{\theta}_1+\dot{\theta}_2+\dot{\theta}_3)\right)^2 + \left(l1c_1\dot{\theta}_1 + l2c_{12}(\dot{\theta}_1+\dot{\theta}_2) + l3c_{123}(\dot{\theta}_1+\dot{\theta}_2+\dot{\theta}_3)\right)^2\right) \tag{17}$$

Where s and c are the sine and cosine functions, respectively. However, the potential energy at each phalange can be obtained as follows:

$$P_i = \frac{1}{2}\sum_1^3(m_i g y_i) \tag{18}$$

Where g is the gravitational constant, and y is the vertical height; thus:

$$P_1 = m_1 g l_1 \sin\theta_1 \tag{19}$$

$$P_2 = m_2 g(l_1\sin\theta_1 + l_2\sin(\theta_1+\theta_2) \tag{20}$$

$$P_3 = m_3 g(l_1\sin\theta_1 + l_2\sin(\theta_1+\theta_2) + l_2\sin(\theta_1+\theta_2+\theta_3) \tag{21}$$

So, the total potential energy of the finger is:

$$P = m_1 g l_1\sin\theta_1 + m_2 g(l_1\sin\theta_1 + l_2\sin(\theta_1+\theta_2) + m_3 g(l_1\sin\theta_1 + l_2\sin(\theta_1+\theta_2) + l_2\sin(\theta_1+\theta_2+\theta_3) \tag{22}$$

Nevertheless, the three phalanges prosthetic finger dynamic can be described by obtaining the Lagrangian using Lagrange Dynamics based on Equation 23, where L is the Lagrangian, K and P are respectively the kinetic and potential finger energies.

$$L = K - P \tag{23}$$

By substituting Equation 17 and 22 in Equation 23 and after simplification will get the Lagrangian as in the equation below:

$$L = 0.5m_1\left(l_1^2\dot{\theta}_1^2\right) + 0.5m_2\left[l_1^2\dot{\theta}_1^2 + l_2^2\left(\dot{\theta}_1^2+\dot{\theta}_2^2+2\dot{\theta}_1\dot{\theta}_2\right) + 2l_1l_2c_2\left(\dot{\theta}_1^2+\dot{\theta}_1\dot{\theta}_2\right)\right] + 0.5m_3\left[l_1^2\dot{\theta}_1^2 + l_2^2\left(\dot{\theta}_1+\dot{\theta}_2\right)^2 + l_3^2\left(\dot{\theta}_1+\dot{\theta}_2+\dot{\theta}_3\right)^2 + 2l_1l_2c_2\left(\dot{\theta}_1^2+\dot{\theta}_1\dot{\theta}_2\right) + l_1l_3c_{23}\left(\dot{\theta}_1+\dot{\theta}_2+\dot{\theta}_3\right)^2 + l_2l_3c_3\left(\dot{\theta}_1+\dot{\theta}_2\right)\left(\dot{\theta}_1+\dot{\theta}_2+\dot{\theta}_3\right) + l_1\dot{\theta}_1^2 + l_2\left(\dot{\theta}_1+\dot{\theta}_2\right)^2 + l_3\left(\dot{\theta}_1+\dot{\theta}_2+\dot{\theta}_3\right)^2\right] - [m_1 g l_1 s_1 + m_2 g(l_1 s_1 + l_2 s_{12}) + m_3 g(l_1 s_1 + l_2 s_{12} + l_2 s_{123})] \tag{24}$$

Using the Lagrange-Euler formulation that is shown in Equation 25 below, the system equations of motion can be obtained for each system coordinate$[\theta_1\ \theta_2\ \theta_2]$, which give the applied torque on each joint, as follows:

$$\frac{d}{dt}\left(\frac{dL}{d\dot{\theta}_i}\right) - \frac{dL}{d\theta_i} = \tau_i \tag{25}$$

$$m_1 l_1^2 \ddot{\theta}_1 + m_2\left[l_1^2\ddot{\theta}_1 + l_2^2(\ddot{\theta}_1+\ddot{\theta}_2) + l_1 l_2 c_2(2\ddot{\theta}_1+\ddot{\theta}_2) - l_1 l_2 s_2(2\dot{\theta}_1\dot{\theta}_2+\dot{\theta}_2^2)\right] + 0.5m_3\left[2l_1^2\ddot{\theta}_1 + 2l_2^2(\ddot{\theta}_1+\ddot{\theta}_2) + 2l_3^2(\ddot{\theta}_1+\ddot{\theta}_2+\ddot{\theta}_3) + 2l_1 l_2 c_2(2\ddot{\theta}_1+\ddot{\theta}_2) - 2l_1 l_2 s_2(2\dot{\theta}_1\dot{\theta}_2+\dot{\theta}_2^2) + 2l_1 l_3 c_{23}(\ddot{\theta}_1+\ddot{\theta}_2+\ddot{\theta}_3) - 2l_1 l_3 s_{23}(2\dot{\theta}_1+2\dot{\theta}_2+\dot{\theta}_3) + l_2 l_3 c_3\left[(\ddot{\theta}_1+\ddot{\theta}_2)+(\ddot{\theta}_1+\ddot{\theta}_2+\ddot{\theta}_3)\right] - l_2 l_3 s_3\dot{\theta}_3(2\dot{\theta}_1+2\dot{\theta}_2+\dot{\theta}_3) + 2l_1\ddot{\theta}_1 + 2l_2(\ddot{\theta}_1+\ddot{\theta}_2) + 2l_3(\ddot{\theta}_1+\ddot{\theta}_2+\ddot{\theta}_3)\right] - [m_1 g l_1 c_1 + m_2 g(l_1 c_1 + l_2 c_{12}) + m_3 g(l_1 c_1 + l_2 c_{12} + l_2 c_{123})] = \tau_1 \tag{26}$$

$$m_2\left[l_2^2(\ddot{\theta}_1+\ddot{\theta}_2) + l_1 l_2 c_2\ddot{\theta}_1 - l_1 l_2 s_2\dot{\theta}_1\dot{\theta}_2\right] + 0.5m_3\left[2l_2^2(\ddot{\theta}_1+\ddot{\theta}_2) + 2l_3^2(\ddot{\theta}_1+\ddot{\theta}_2+\ddot{\theta}_3) + 2(l_1 l_2 c_2\ddot{\theta}_1 - l_1 l_2 s_2\dot{\theta}_1\dot{\theta}_2) + 2l_1 l_3 c_{23}(\ddot{\theta}_1+\ddot{\theta}_2+\ddot{\theta}_3) - 2l_1 l_3 s_{23}(\dot{\theta}_1+2\dot{\theta}_2+2\dot{\theta}_3) + l_2 l_3 c_3(2\ddot{\theta}_1+2\ddot{\theta}_2+\ddot{\theta}_3) - l_2 l_3 s_3\dot{\theta}_3(2\dot{\theta}_1+2\dot{\theta}_2+\dot{\theta}_3) + 2l_2(\ddot{\theta}_1+\ddot{\theta}_2) + 2l_3(\ddot{\theta}_1+\ddot{\theta}_2+\ddot{\theta}_3)\right] - 2l_1 l_2 s_2(\dot{\theta}_1^2 + \dot{\theta}_1\dot{\theta}_2) - 0.5m_3\left[2l_1 l_2 s_2\dot{\theta}_1(\dot{\theta}_1+\dot{\theta}_2) + l_1 l_3 s_{23}(\dot{\theta}_1+\dot{\theta}_2+\dot{\theta}_3)^2\right] - [m_2 g(l_2 c_{12}) + m_3 g(l_2 c_{12} + l_2 c_{123})] = \tau_2 \tag{27}$$

$$0.5m_3\left[2l_3^2(\ddot{\theta}_1+\ddot{\theta}_2+\ddot{\theta}_3) + 2l_1 l_3 c_{23}(\ddot{\theta}_1+\ddot{\theta}_2+\ddot{\theta}_3) - 2l_1 l_3 s_{23}(\dot{\theta}_1+2\dot{\theta}_2+2\dot{\theta}_3) + l_2 l_3 c_3(\ddot{\theta}_1+\ddot{\theta}_2) - l_2 l_3 s_3\dot{\theta}_3(\dot{\theta}_2+\dot{\theta}_3) + 2l_3(\ddot{\theta}_1+\ddot{\theta}_2+\ddot{\theta}_3)\right] - 0.5m_3\left[l_1 l_3 s_{23}(\dot{\theta}_1+\dot{\theta}_2+\dot{\theta}_3)^2 - l_2 l_3 s_3(2\dot{\theta}_1+2\dot{\theta}_2+\dot{\theta}_3)\right] - [m_3 g(l_3 c_{123})] = \tau_3 \tag{28}$$

Where τ_i is the torque that each phalange experiences, and $\ddot{\theta}$ is the angular acceleration? However, the system generalized equations of motion in the matrix form is given by the following nonlinear form:

$$M(\theta)\,\ddot{\theta} + V(\theta,\dot{\theta}\,) + G(\theta) = \tau \tag{29}$$

Where $M(\theta)$ is an 3×3 mass matrix, $V(\theta,\dot{\theta}\,)$ is an 3×1 vector contains the Coriolis and centrifugal terms, $G(\theta)$ is an 3×1 gravity vector, and τ is an 3×1 generalized input torque vector;

$$\begin{bmatrix} M_{11} & M_{12} & M_{13} \\ M_{21} & M_{22} & M_{23} \\ M_{31} & M_{32} & M_{33} \end{bmatrix}\begin{bmatrix} \ddot{\theta}_1 \\ \ddot{\theta}_2 \\ \ddot{\theta}_3 \end{bmatrix} + \begin{bmatrix} VG_1 \\ VG_2 \\ VG_3 \end{bmatrix} = \begin{bmatrix} \tau_1 \\ \tau_2 \\ \tau_3 \end{bmatrix} \tag{30}$$

The terms VG_1, VG_2 and VG_3 constitute the lumped expressions of Carioles/centrifugal forces and gravity consequences. We assume that phalange 1 is attached to phalanges 2 and 3 through the pulley-belt machine approach.

3. Classical sliding mode controller (SMC)

One of the successful methods to monitor nonlinear systems involving matched disturbances is sliding mode control (SMC), which has provided efficiency in design has been widely used in industrial[7]. In this control scheme, states of the system are handled toward a sliding surface and forced to stay on (or near) it. However, two parts are there within the layout of this class of controllers. Firstly, within the system's state space model, a sliding surface is introduced; secondly, to construct and maintain the sliding motion, the control law, which is responsible for that, is found [8]. Thus, the sliding surface (s) can be presented as:

$$s = \lambda e + \dot{e} = 0 \tag{31}$$

Where λ is a constant and it is > 0. However, let assume that $x_1 = e, x_2 = \dot{e}$ where e is the error and $\dot{e}$ is the dervitive of the error and$\lambda = 1$, hence the sliding surface can be rewritten as:

$$s = x_1 + x_2 \tag{32}$$

The complete control law can be defined as follows:

$$u = u_n + u_{dis} \tag{33}$$

Where, u_n represent the nominal control part, and u_{dis} the discontinuous control part [9], which is defined as:

$$u_{dis} = -k(x)sign(s) \tag{34}$$

K (x) is a discontinuous gain, and $sign\ (s)$ is known as a signup function, which can mathematically be expressed as in Equation 35 below.

$$sign(s) = \begin{cases} 1 & if\ s > 0 \\ -1 & if\ s < 0 \\ 0 & if\ s = 0 \end{cases} \quad (35)$$

Therefore, the control action equation can be written as [10]:

$$u = u_n - k(x)sign(s) \quad (36)$$

The structure of the SMC is shown in Figure 4. This structure has one input: the motor's torque and the output is the finger's desired position. To reduce the chattering problem, the saturation function is used instead of $sign\ (s)$ function in Equation 36; thus, it can be rewritten as:

$$u = u_n - k(x)sat(s) \quad (37)$$

Where the saturation function is:

$$sat(s.\varphi) = \begin{cases} sign(s) & if\ |s| > \varphi \\ \frac{s}{\varphi} & if\ |s| \leq \varphi \end{cases} \quad (38)$$

Where φ expresses the boundary layer's width, as shown in Figure 5 (saturation function).

4. Adaptive Sliding Mode Control (ASMC) Design

The biggest challenges to applying SMC scheme are two interrelated phenomena: chattering and high control action activity. The amplitude of the chattering is proportional to the magnitude of the discontinuous total control. These two issues can be solved at the same time if the magnitude is decreased to a minimum permissible level represented by the conditions for the existing sliding mode [9]. In this study, ASMC is proposed to deal with the two issues mentioned above. ASMC has repressed the switching gain to a low level. When the gains are decreased, the effects of control actions are minimized, which causes attenuating the chattering. Reduce the chattering leads to good tracking performance, which is decreasing the thermal and mechanical losses in the systems [11].The ASMC is more compact and relaxed in the architecture than the classical SMC. As well as, the system reliability is achieving with a limited control effort while using the ASMC[12].

$$u = -k(t)\text{sign}(s) \quad (39)$$

Where, u is the control action to be configured, and *k (t)* is the adaptive controller gain that is described as in the following:

$$k(t) = \begin{bmatrix} k_1(t) \\ k_2(t) \\ k_3(t) \end{bmatrix} \quad (40)$$

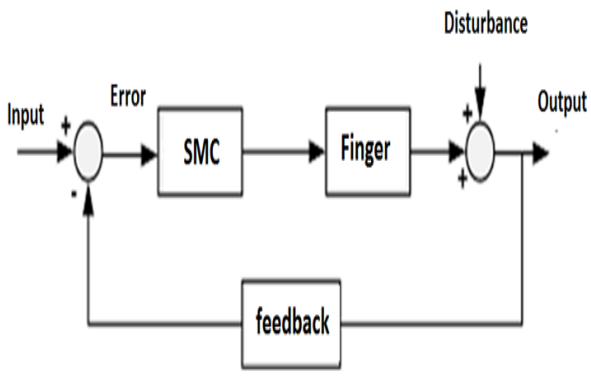

Figure 1: Block diagram of the prosthetic finger with control

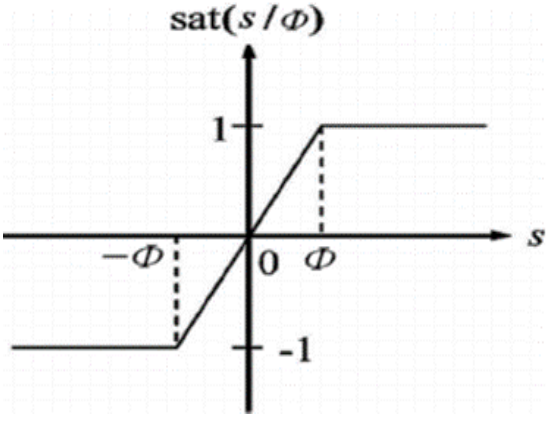

Figure 2: Saturation function

Table 1: The Symbol definition

Symbol	Definition	Unit
τ	Torque	N.m
s	Sliding surface	---
λ	Sliding manifold slope	---
$e, \dot{e}$	the error and is the derivative of the error respectively	---
φ	The width of the boundary layer	---
ρ	Modification gain	---

And $s = \begin{bmatrix} s_1 \\ s_2 \\ s_3 \end{bmatrix}$ is the sliding variable, and sign (s) is the signup function previously described in Equation 35. The quantification of the adaptive controller gain is as below [13] :

$$\dot{\mu} = \{\rho|s(x,t)|\text{sign}(|s(x,t)| - \epsilon) \tag{41}$$

Where $\mu = \begin{bmatrix} \mu_1 \\ \mu_2 \\ \mu_3 \end{bmatrix}$, $\rho > 0$ and $\epsilon > 0$, and *k(t)* is chosen depending on the following rules [11].

$$k = \begin{cases} \mu & \text{if Kmin} < \mu < \text{Kmax} \\ \text{Kmin} & \text{if } \mu \leq \text{Kmin} \\ \text{Kmax} & \text{if } \mu \geq \text{Kmax} \end{cases} \tag{42}$$

Where $\text{Kmin} < \big(\mu(0) = k(0)\big) < \text{Kmax}$.

$Kmin$ is the lowest acceptable value of *k(t), Kmax* the highest acceptable value of *k(t)* can the system handle it, and μ (0) is the initial start point of the gain k(t). To provide more information and illustrations on the rule of the adaptive control and how to apply the conditions of Equation 42, the following flowchart is presented.

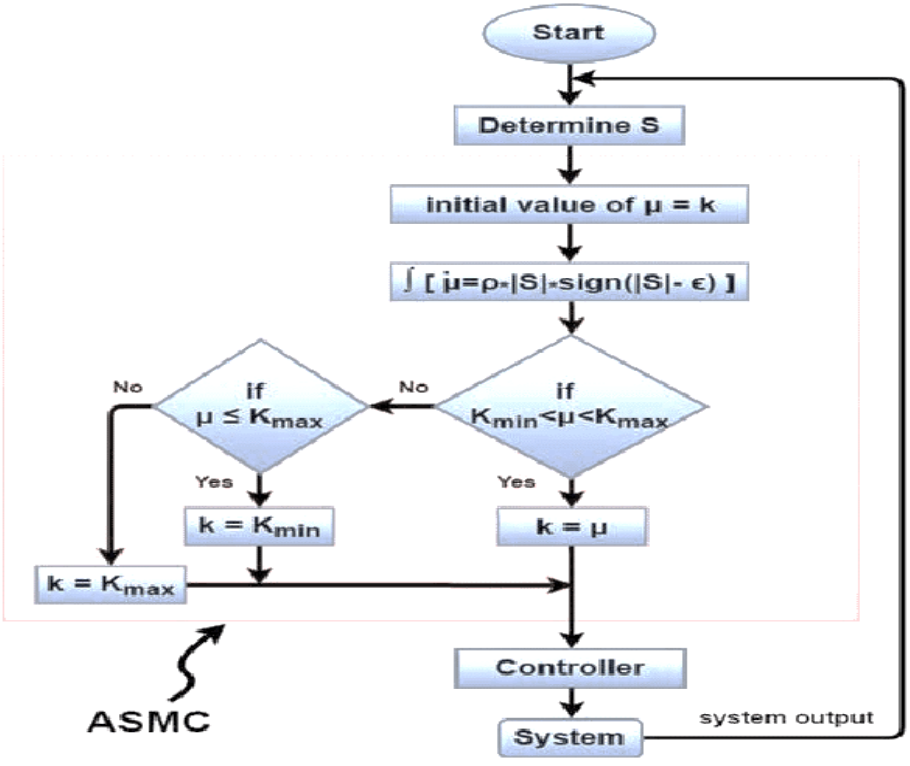

Figure 3: Flow chart algorithm of ASMC

Finally, the controller law will be updated with a saturation function as opposed to the signup function, as described:

$$u = -k(t)\text{sat}(s, \varphi) \tag{43}$$

The main purpose of the ASMC technique is to design a robust controller that can be able to Orient the sliding variable toward the manifold surface and keep the system trajectory in this required sliding surface[14].

5. Simulation Results

In this work, two techniques were used to control a prosthetic finger. In the current simulation results, the adaptive sliding mode control shows more effectiveness than the classical sliding mode control by solving the chattering problem concerned with high control effort and high control gain. The system has been simplified into six states, which have the initial states as follow:

$$x_1(0) = \frac{\pi}{4}(\text{rad}), x_2(0) = \frac{\pi}{4}(\text{rad}), x_3(0) = \frac{\pi}{4}(\text{rad}), x_4(0) = 0\left(\frac{\text{rad}}{\text{sec}}\right), x_5(0) = 0\left(\frac{\text{rad}}{\text{sec}}\right), x_6(0) = 0\left(\frac{\text{rad}}{\text{sec}}\right) \quad (44)$$

Wherex_1, x_2 and x_3 are the postion of the three phalanges and x_4, x_5 and x_6 are the velocity. The parameter values are presented in Table 2. Figures 6 and 7 illustrate the state of trajectory from the initial to the end point for the three phalanges. Using the reaching condition of SMC. These trajectories reach approximately zero, and it will make the system asymptotic stable. Figures 8 and 9 show the tracking performance between the actual and desired position, which does not exceed 2.5 sec for both CSMC and ASMC. Figures 10 - 11 show the sliding variables for the three-phalange; it is clear that the CSMC suffers from some chattering issue, while the ASMC has a smooth sliding surface. Figure 12 illustrates the control gain for both CSMC and ASMC; the ASMC can reduce the gain to an acceptable value compared with CSMC, where the high gain value is the reason for high charting in the torque action. Figure 13 shows the torque action for the CSMC and ASMC; however, it is evident that utilizing the CSMC on the system, the model will suffer from chattering while applying the ASMC minimizes the chattering phenomenon.

Table 2: The model parameters

Parameter	Definition	Units
L1	Length of phalange 1	m
L2	Length of phalange 2	m
L3	Length of phalange 3	m
m1	Mass of phalange 1	Kg
m2	Mass of phalange 2	Kg
m3	Mass of phalange 3	Kg
θ1 desired	The desired angle for phalange 1	rad
θ2 desired	The desired angle for phalange 2	rad
θ3 desired	The desired angle for phalange 3	rad
G	Gravitational constant	m/s^2
d	Disturbance	N.m
Φ	Boundary layer width	--

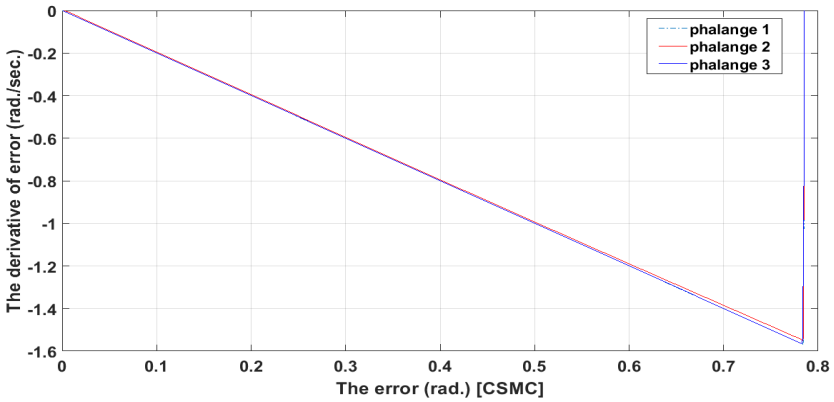

Figure 4: The phase plane trajectory of CSMC

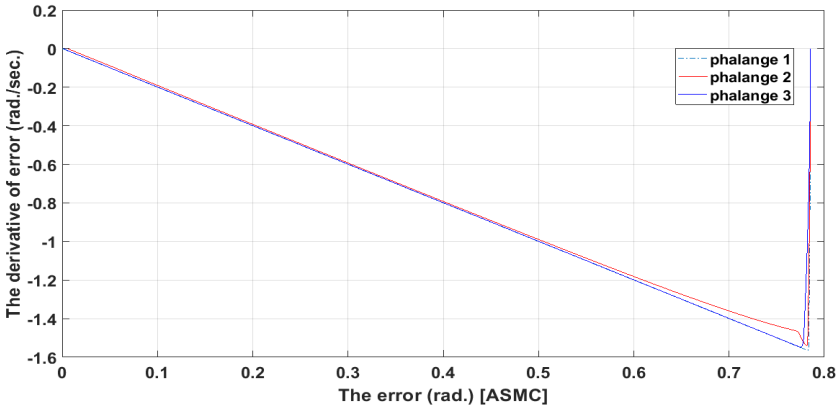

Figure 5: The phase plane trajectory of ASMC

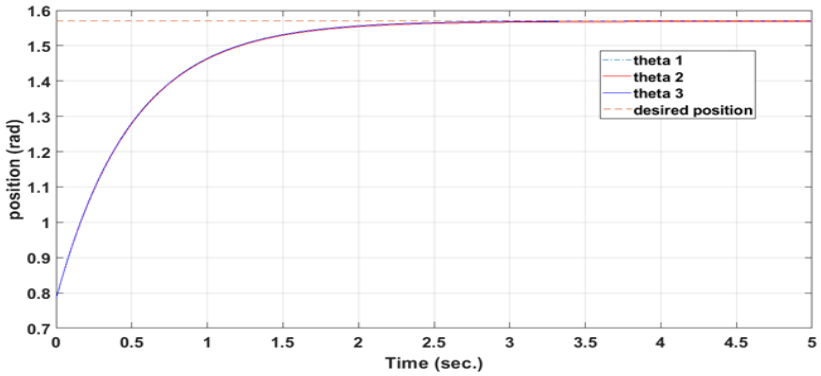

Figure 6: The performance of tracking between the desired and existing position of CSMC

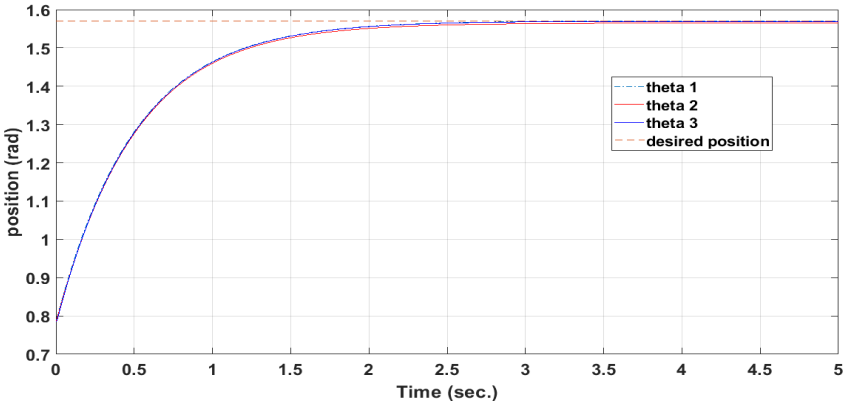

Figure 7: The performance of tracking between the desired and existing position of ASMC

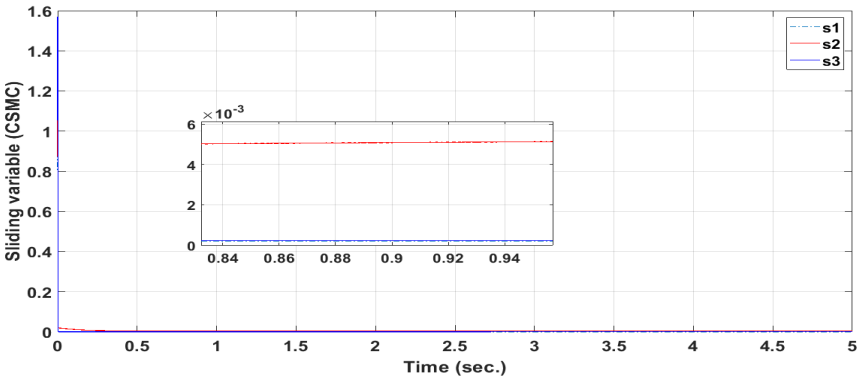

Figure 8: Sliding variable of CSMC

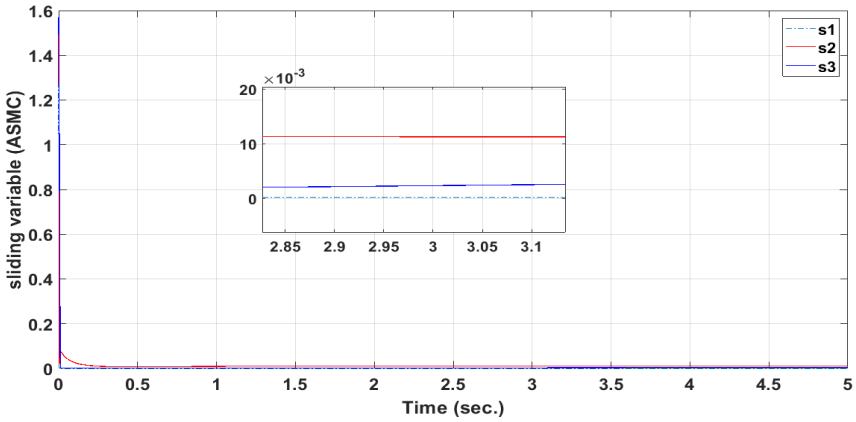

Figure 9: Sliding variable of ASMC

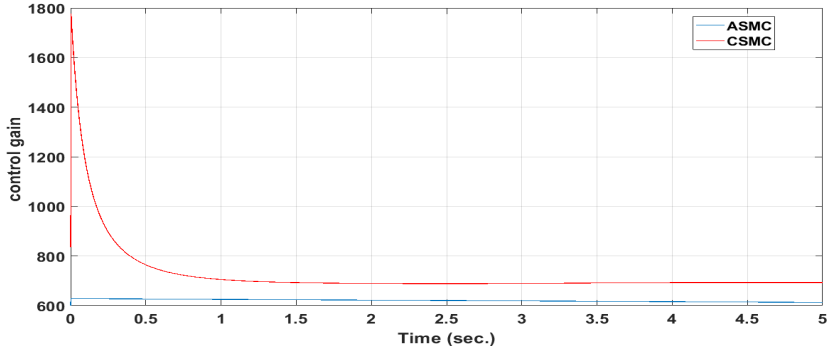

Figure 10: Control gain for both CSMC and ASMC

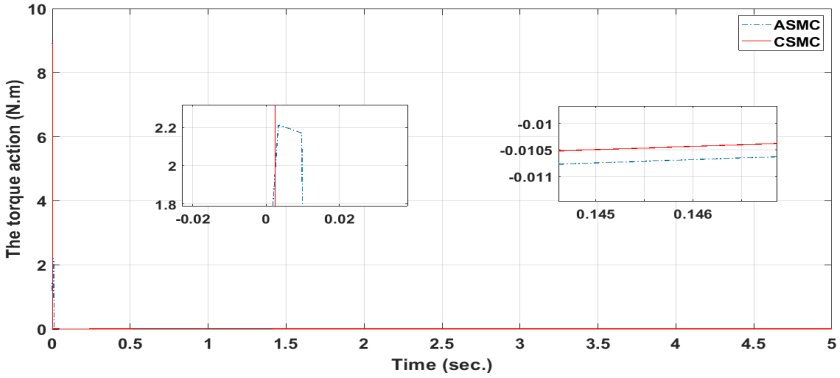

Figure 11: Control action for both CSMC and ASMC

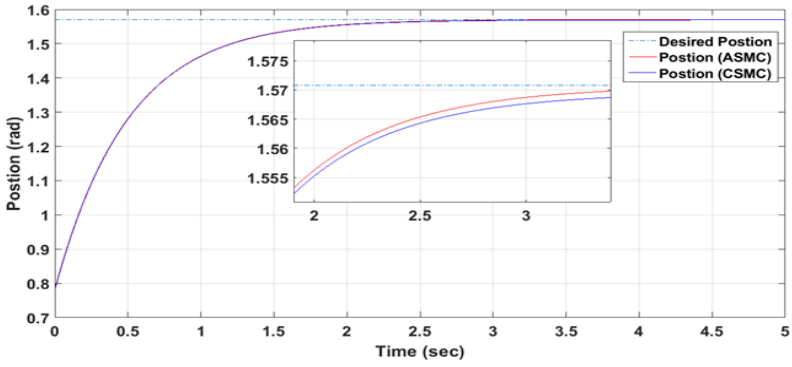

Figure 12: Error between desired and real for both CSMC and ASMC

6. Conclusions

The modeling and control of a tendon controlled 3-degree of freedom prosthetic finger was presented in this research. After obtaining the dynamic modeling, the classic (CSMC) and adaptive (ASMC) sliding mode control techniques were then

applied to control the finger's motion. It was noticed that the chattering phenomenon is a severe problem of CSMC. However, the comparison between the CSMC and ASMC which is clarified in Table 3, demonstrated that the ASMC could reduce the controllers' gain value to be reasonable and minimal, thus reducing the control and chattering magnitude. It was also concluded that the ASMC reduces the gain to an acceptable value compared with CSMC, which produces high gain leading to high chattering in the torque action. This was evident from the obtained results where the model system suffered from chattering while applying the ASMC minimizes the chattering phenomenon.

Table 3: The performance and the characteristics of the CSMC and ASMC

Control	Maximum Control gain k(t)	maximum chattering magnitude (N.m)	The steady-state error
CSMC	0.0013	8.9	1775.1
ASMC	0.0005	2.2	628.25

Author contribution

All authors contributed equally to this work.

Funding

This research received no specific grant from any funding agency in the public, commercial, or not-for-profit sectors.

Data availability statement

The data that support the findings of this study are available on request from the corresponding author.

Conflicts of interest

The authors declare that there is no conflict of interest.

References

[1] B. Sharma, M. Kiran, V. Siva, B. Rama, S. Joshi, Mathematical Modeling and Design Analysis of a Dexterous End-effector, Int. j. eng. res., 1(2012) 01-08.

[2] N. S. Pollard , R. C. Gilbert, Tendon arrangement and muscle force requirements for human-like force capabilities in a robotic finger , IEEE Int.Conf., 4 (2016). http://dx.doi.org/10.1109/ROBOT.2002.1014298

[3] M. V. Weghe, M. Rogers, M. Weissed, Y. Matsuokal, the ACT Hand : Design of the Skeletal Structure, IEEE Int. Conf. Robot., 4 (2004) 3375–3379. http://dx.doi.org/10.1109/ROBOT.2004.1308775

[4] S. Aluminium, I. Co, A. Science, Position and Elasticity Control for Biomimetic Robot Finger, (2000) 870–875.

[5] D. Hristu, J. Babb, H. Singh, S. Gottschlich, Position and Force Control of a Multifingered Hand : A Comparison of Fuzzy Logic to Traditional PID Control, IEEE Int. Workshop Conf. Intell. Robots. Syst., 2 (1994) 1391–1398. http://dx.doi.org/10.1109/IROS.1994.407502

[6] A. C. Escamilla, J. F. G. Aguilar, M. G. L. López, V. M. A. Martínez, G. V. G. Ramírez, Triple pendulum model involving fractional derivatives with different kernels, Chaos. Solit., 91 (2016) 248–261. http://dx.doi.org/10.1016/j.chaos.2016.06.007

[7] A. F. Abd ,S. A. Al-Samarraie, Integral Sliding Mode Control Based on Barrier Function for Servo Actuator with Friction, Eng. Technol. J., 39 (2021) 248–259. http://dx.doi.org/10.30684/etj.v39i2a.1826

[8] N. Yagiz, Y. Z. Arslan, Y. Hacioglu, Sliding mode control of a finger for a prosthetic hand, J. Vib. Control., 13 (2007) 733–749.

[9] Y. Shtessel, C. Edwards, L. Fridman, A. Levant, Sliding Mode Control and Observation, Control Eng., (2014) 356. http://dx.doi.org/10.1007/978-0-8176-4893-0

[10] P. Taylor, Tracking control of non-linear systems using sliding surfaces, with application to robot manipulators, (2013), (2007) 37–41.

[11] S. Ahmed , M. M. Salih, Adaptive Sliding Mode Control for Robotic System with Unknown Deadzone and LuGre friction , Int. Conf. Recent .Trends. Eng. Sci. Sustain., 2018 (2017) .

[12] D. H. Tohma , A. K. Hamoudi, Design of Adaptive Sliding Mode Controller for Uncertain Pendulum System, Eng. Technol. J., 39 (2021) 355–369. http://dx.doi.org/10.30684/etj.v39i3a.1546

[13] P. Ignaciuk , A. Bartoszewicz, Advances in Sliding Mode Control, 440 (2013).

[14] S. A. Hashim , A. K. Hamoudi, Design a Second Order Sliding Mode Controller for Electrical Servo Drive Systems, Eng. Technol. J., 37 (2019) 542-552. http://dx.doi.org/10.30684/etj.37.12A.8